Neotectonic development of the Çameli Basin, southwestern Anatolia, Turkey

MEHMET CIHAT ALÇIÇEK[1], JOHAN H. TEN VEEN[2,3] & MEHMET ÖZKUL[1]

[1]*Department of Geological Engineering, Pamukkale University, 20070 Denizli, Turkey (e-mail. alcicek@pamukkale.edu.tr)*

[2]*Faculty of Earth and Life Sciences, Free University, de Boelelaan 1085, 1081 HV Amsterdam, Netherlands*

[3]*Institute for Geology, Mineralogy and Geophysics, Universitätsstrasse 190, D-44-801, Bochum, Germany*

Abstract: This study of the Çameli Basin presents a detailed basin evolution combined with structural analysis and provides the first detailed time–stratigraphic framework for the neotectonic development of Neogene grabens along the Fethiye–Burdur Fault Zone in southwestern Anatolia. During the Early Tortonian, the Çameli Basin was established as a broad fault-bounded fluviolacustrine basin that experienced NW–SE extension. By Mid-Pliocene time, continued NW–SE extension resulted in the formation of a new intrabasinal fault zone that split the basin longitudinally into two compartments. The development of a new generation of normal faults further split the basin into four narrow half-graben compartments at the end of the Late Pliocene. Structural analysis of basin-bounding and intrabasinal faults related to this three-stage basin development shows that NW–SE extension apparently persisted from Late Miocene to early Quaternary time. The youngest (i.e. Holocene), deformation is characterized by dextral shear along NE–SW-trending strike-slip faults and continuing NW–SE extension. The Late Miocene foundering of the basin was related to extension in the northerly hinterland zone of the still-emplacing Lycian nappes, whereas outward growth of the Hellenic Arc in response to the westward Anatolian extrusion is the main cause for NW–SE extension from the Pliocene onward. Dextral strike-slip faulting is localized and is associated with the activity of NW–SE-trending faults that accommodated NE–SW extension. The simultaneous activity of these faults suggests the existence of biaxial extensional tectonics, as initially proposed for the Burdur–Dinar area. Sinistral strike-slip faulting, continuing along the eastern Hellenic Arc, penetrated the southernmost part of Turkey but has not yet reached the Çameli Basin area. Our biostratigraphically well-constrained tectonosedimentary model for the evolution of the Çameli Basin provides a reliable time-stratigraphic framework for NE–SW extension in the 'Fethiye–Burdur Fault Zone' of SW Anatolia. We believe that this fault zone represents a broad zone of isolated or interconnected NE–SW-trending basins that formed under prevailing NW–SE extension, rather than being a significant strike-slip fault zone.

Regional-scale tectonic extension has influenced the development of numerous fault-bounded intramontane basins in southwestern Anatolia. This extension follows the final stages of the Late Cretaceous–Miocene Tethys ocean closure and formation of the Tauride orogen (Şengör & Yılmaz 1981; Robertson & Dixon 1984; Şengör *et al.* 1985; Zanchi *et al.* 1993). Three tectonic provinces can be distinguished in SW Anatolia (Fig. 1): (1) the eastern Aegean extensional province; (2) the Isparta Angle; (3) the Fethiye–Burdur Fault Zone that geographically connects the former two (Fig. 1). In the eastern Aegean extensional province (EAEP) extension is characterized by basins with a general NE–SW and east–west orientation, which are commonly referred to as cross-grabens (Şengör 1987). The cause(s) and timing of the crustal extension are subjects of continuing debate and, until now, remain controversial (Yılmaz *et al.* 2000; Bozkurt 2001, 2003). For several basins in the EAEP, Purvis & Robertson (2004, 2005*a*,*b*) have presented new field-based evidence and Ar–Ar dating that support a three-phase 'pulsed extension' model. A presumably Late Oligocene phase of extensional unroofing of the Menderes Metamorphic Massif created approximately NE–SW scoop-shaped depressions. The major east–west-trending grabens foundered during an Early–Late Miocene phase of north–south extension related to rollback of the Aegean subduction zone. This interpretation concurs with

From: ROBERTSON, A. H. F. & MOUNTRAKIS, D. (eds) 2006. *Tectonic Development of the Eastern Mediterranean Region*. Geological Society, London, Special Publications, **260**, 591–611.
0305-8719/06/$15.00

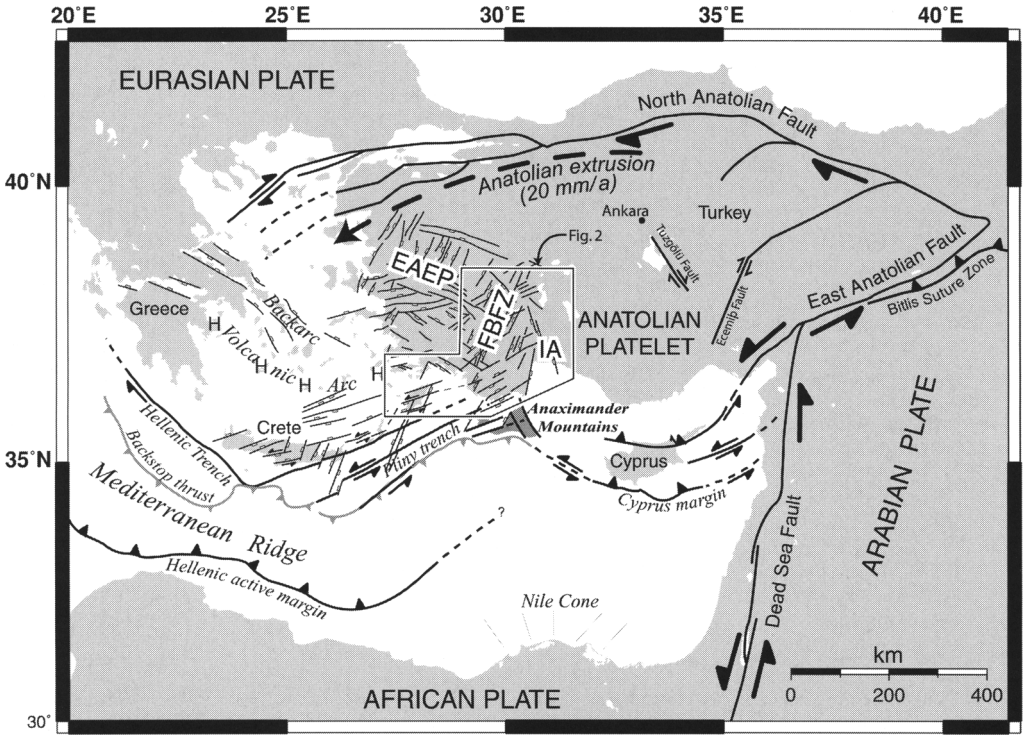

Fig. 1. Geodynamic framework of the eastern Mediterranean showing main structural features in the Hellenic Arc and southwestern Turkey with its three tectonic provinces: EAEP, eastern Aegean extensional province; FBFZ, Fethiye–Burdur Fault Zone; IA, Isparta Angle. Box shows location of Figure 2.

that of the evolution of other Miocene basins in the Aegean region such as Crete (ten Veen & Postma 1999) and Rhodes (ten Veen & Kleinspehn 2002). A young Pliocene–Quaternary phase of north–south extension in the EAEP is related to westward tectonic escape of Anatolia.

Recent studies by Flecker *et al.* (1995, 2005) and Glover & Robertson (1998) have revealed the complex Miocene–Recent tectonic evolution of the Isparta Angle (Figs 1 and 2). Fault orientations in the Isparta Angle are NE–SW, NW-SE to north–south, and slicken-fibre patterns indicate multiple fault reactivations. Reverse faulting took place under compression during the Late Miocene Aksu phase and right-lateral strike-slip faulting occurred during latest Miocene–earliest Pliocene transtension. In the Late Pliocene–early Pleistocene, approximate east–west extension formed the present Aksu Basin as a north–south half-graben in the core of the Isparta Angle. The onset of this extension is thought to be related to a regional change in stress direction in the Aegean region (Glover & Robertson 1998), plausibly related to the onset of westward tectonic escape of Anatolia.

The Fethiye–Burdur Fault Zone (FBFZ) is characterized by the dominance of Late Miocene–Quaternary NE–SW-trending faults and basins. These occur in a roughly linear arrangement between Fethiye and Afyon and include the Çameli, Burdur, Acıgöl, Sandıklı, Çivril and Eşen Çay basins and their bounding faults (Fig. 2). To the north the FBFZ merges with a series of WNW–ESE grabens, including the Dinar, Beyşehir, Akşehir–Afyon and Dombayova grabens and their bounding faults. The latter are interpreted as the easternmost expression of the east–west basins of the Aegean extensional province (Westaway 1990), or as a westernmost part of a reactivated Aksu thrust fault (Temiz *et al.* 1997). Many earthquakes originate from both of these WNW- and NE-trending structures, including the 3 October 1914 Burdur ($M=7.1$), 7 August 1925 Dinar ($M=5.8$), 19 July 1933 Çivril ($M=5.8$), 12 May 1971 Burdur ($M=6.2$), 1 October 1995 Dinar ($M=6.1$) and 15 December 2000 Akşehir ($M=5.8$) earthquakes. Some workers (e.g. Dumont *et al.* 1979; Eyidoğan & Barka 1996; Barka *et al.* 1997) have suggested that the FBFZ

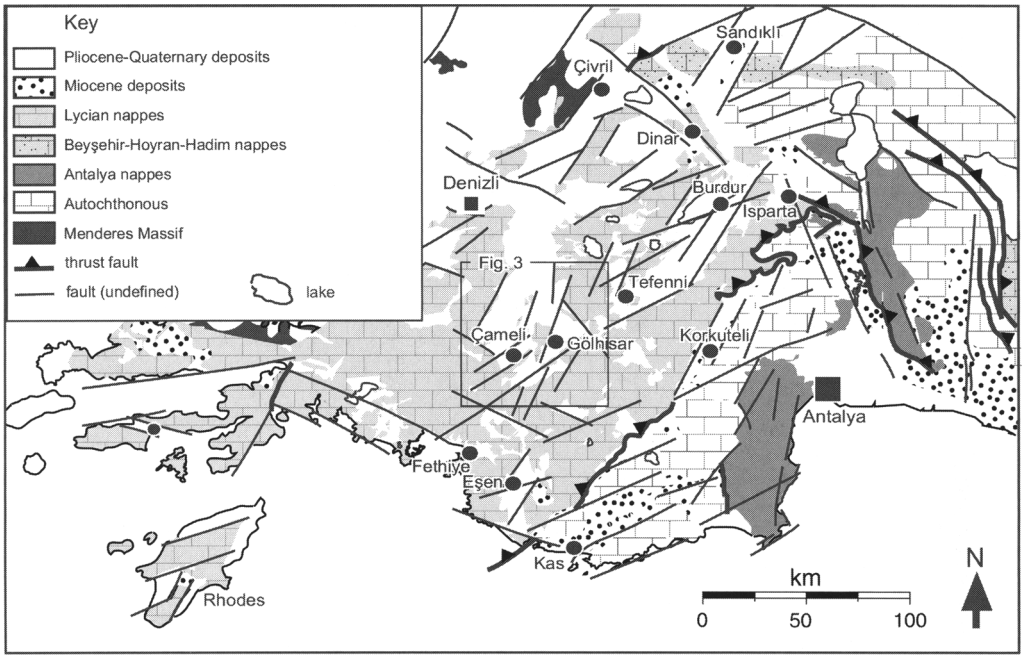

Fig. 2. General geological map of southwestern Turkey, including the FBFZ and the Isparta Angle (based on Şenel 1997*a–f*), showing major lineaments detectable in satellite imagery (ASTER) and digital terrain models (GTOPO30). Main structural features in the Isparta Angle are after Glover & Robertson (1998).

represents a regionally important sinistral, transtensional fault. However, sinistral strike-slip motions are not evident from earthquake focal mechanisms (Taymaz *et al.* 1991; Taymaz & Price, 1992), and Koçyiğit *et al.* (2000) regarded it as a normal fault zone. The interpretation that the FBFZ is a continuation of the sinistral Pliny fault zone (Barka *et al.* 1997; Alçiçek *et al.* 2002) has been put in doubt by ten Veen *et al.* (2004), who showed that the Pliny 'trench' in fact continues in offshore southern Turkey (Fig. 1).

As shown in Figure 2, NE–SW-trending faults occur not only along a zone from Fethiye to Burdur, but are numerous throughout southwestern Turkey. Although these faults are the most pronounced features, the actual geometries of the basins in this area appear to be related to a combination of NE–SW and north–south faults. This en echelon basin configuration becomes apparent on satellite images, such as for the Eşen Çay Basin (see ten Veen 2004; Fig. 2), and in multibeam bathymetry images of the Anaximander Mountains, offshore southern Turkey (ten Veen *et al.* 2004; Fig. 1). This fault pattern continues westwards into the eastern Hellenic Arc, where deformation occurs as a result of a transtensional setting (e.g. ten Veen & Kleinspehn 2002, 2003). A limited number of structural analyses in SW Turkey (e.g. Dumont *et al.* 1979; Temiz *et al.* 1997, 2001) indicate the presence of normal, oblique and strike-slip faults, and several conflicting regional interpretations have emerged from fault kinematic analyses of these faults. For the Eşen Çay Basin (Fig. 2), structural and sedimentological data indicate that the Plio-Pleistocene period was marked by east–west to WNW–ESE extension, but the Holocene–Recent period was characterized by a complex combination of faults of which sinistral strike-slip faults trending 070° are the most important. Fault-slip analysis suggests that deformation occurred in a transtensional setting involving the time-transgressive addition of a sinistral shear component, which was possibly produced by northeastward propagating transcurrent motion of the Hellenic forearc (ten Veen 2004).

Thus, it appears that the FBFZ is situated between a zone of north–south neotectonic extension in the EAEP, a zone of transtension along the eastern Hellenic Arc, and a zone of east–west extension in the Isparta Angle. To what extent these geodynamic driving forces play a role in the neotectonic evolution of the study area is still

unclear, as is the role of any sinistral motion along the hypothetical FBFZ.

The present study documents the tectonosedimentary evolution of the Late Miocene–Late Pliocene, intramontane Çameli Basin in the central part of the FBFZ (Fig. 1), based on sedimentary facies analysis, biostratigraphic dating and structural analysis. We use the basin fill for temporal and palaeogeographical control in order to document internal basin deformation and adjacent basement kinematics that are related to regional driving mechanisms.

Çameli Basin

The Çameli Basin (Fig. 3), *c.* 40 km wide and 60 km long, consists of a series of NNE–SSW-trending interconnected tilt-block compartments within the Lycian nappes (de Graciansky 1972). Locally, these ophiolite and limestone thrust-sheets are unconformably overlain by Lower Miocene deposits that were first interpreted by Altınlı (1955) as marine-fossiliferous unit. These deposits comprise alluvial red beds overlain by shallow-marine sandstones, marls and fossiliferous limestones. Similar basal sediments, elsewhere in the Lycian nappes, were interpreted as syn-nappe emplacement units by Collins & Robertson (2003). This supra-allochthonous sedimentary cover is here regarded as part of the basement succession (Figs 3, 4; Alçiçek *et al.* 2005).

Along the SE and NW margins, the Dirmil and Bozdağ faults (Fig. 3), respectively, are the main basin-bounding normal faults that delimit the extent of the Çameli Formation. Northwest-dipping secondary normal faults divide the basin into four approximately equal-sized compartments (Fig. 5). Although the Çameli Basin is part of a larger area of NNE–SSW-trending basins that constitute the hypothetical FBFZ, the individual basin-bounding faults do not extend beyond the basin's northern and southern limits. Instead, NW–SE-trending faults delimit the basin and there is no evidence of cross-cutting fault relationships. Counterparts of the ENE–WSW lineaments, which are clear from satellite imagery and terrain models (Fig. 2) are not observed as basin-scale faults in the Çameli area.

The deposits of the Çameli Formation exhibit a general southeastward dip towards the NW-dipping faults (Fig. 3) and are unconformably overlain by non-tilted Quaternary alluvial deposits, which are generally <20 m in thickness. The Çameli Formation was originally mapped as the 'Neogene cover' of the Lycian nappes and assumed to be Pliocene in age (Becker-Platen 1970; Erakman *et al.* 1982; Meşhur & Akpınar 1984), although it was neither dated nor sedimentologically studied. More recently, the age of the Çameli Formation has been determined as Late Miocene (Tortonian) to Late Pliocene (Gelasian) based on terrestrial mammal macro- and microfossils and molluscan remains (Alçiçek *et al.* 2005). The succession has been grouped into three lithostratigraphic subunits referred to as the Derindere, Kumafşarı and Değne Members, which consist of alluvial-fan, fluvial and lacustrine deposits, respectively. In the central part of the basin, these members overlie each other in a 500 m thick sequence, but they are laterally equivalent along the basin margins (Fig. 3; Table 1; Alçiçek 2001; Alçiçek *et al.* 2004, 2005).

The Derindere Member is composed of coarse-grained alluvial deposits and typically occurs in the lowermost and uppermost parts of the basin fill, especially along the basin margins. This member is 40–60 m thick, dark red in colour and composed of matrix-supported conglomerates and mudstones. The unit passes laterally and vertically into the fluvial Kumafşarı member and the lacustrine Değne Members, and is often found in faulted contact with basement rocks.

The Kumafşarı Member is widespread in the northern part of the basin and in the middle stratigraphic level of the basin fill. The unit consists of up to 146 m of stacked fluvial deposits characterized by a light yellow colour. The unit passes laterally and vertically into the alluvial Derindere and lacustrine Değne members.

The Değne Member is represented by a sequence of lacustrine deposits that varies in thickness between 75 and 300 m. The unit is most common in the southern parts of the basin and mainly constitutes the upper part of the basin succession. The member passes laterally and vertically into the fluvial Kumafşarı Member and the alluvial Değne Member, but is also found resting directly on the basement rocks.

Basin evolution

Stage 1: opening of the Çameli Basin (Late Miocene)

The mammal remains of *Perissodactyla* found in the lowermost part of the basin-fill succession near Elmalıyurt (Figs 3 and 5) indicate that sedimentation in the Çameli Basin commenced by Vallesian time (Early Tortonian 10.8–8.5 Ma; Alçiçek *et al.* 2005). At that time, an ephemeral-lake environment existed along the basin axis, represented by the lacustrine deposits of the Değne Member. Axial-fluvial systems of the Kumafşarı Member supplied sediment

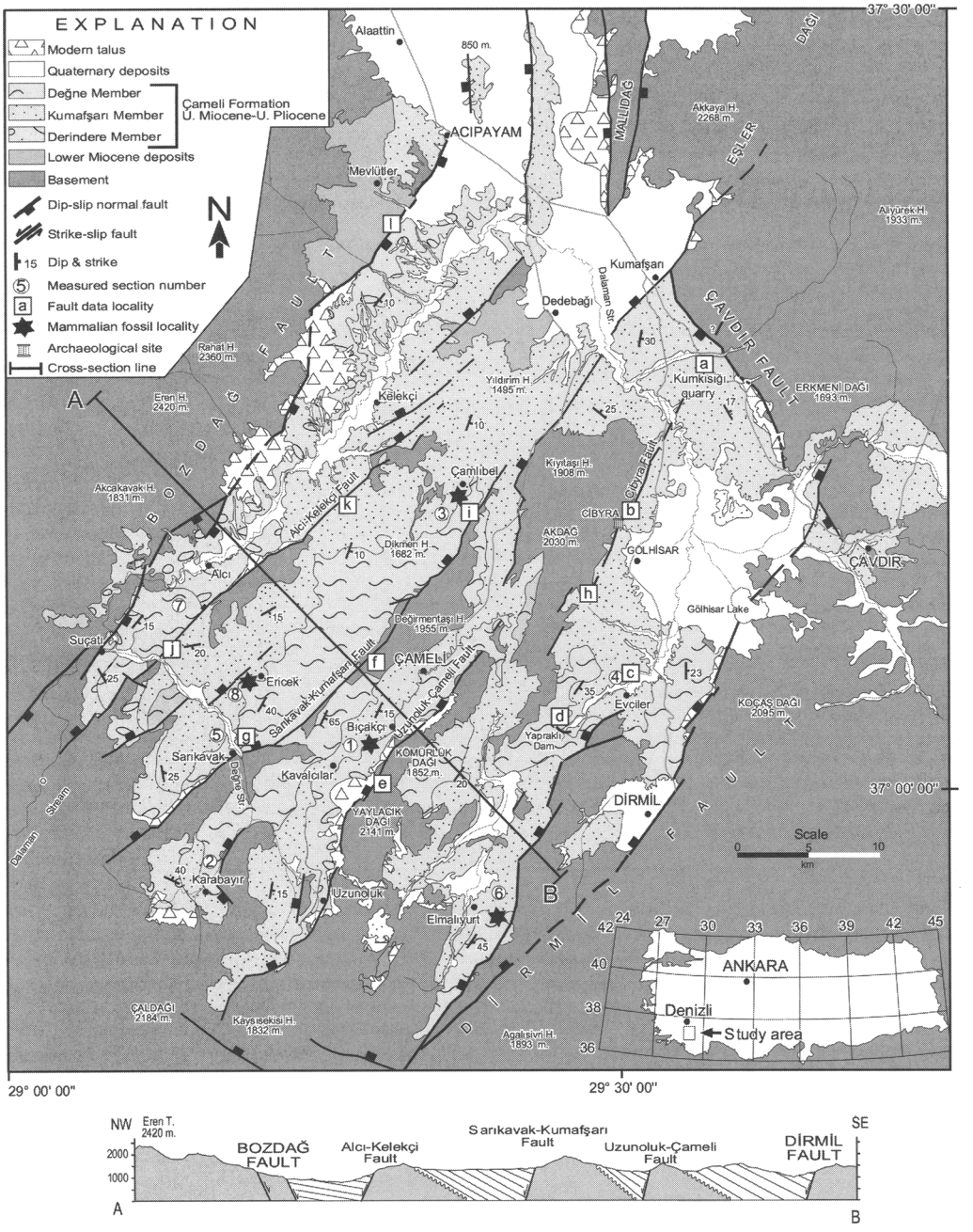

Fig. 3. Geological map and cross-section of the Çameli Basin (modified from Alçiçek *et al.* 2005).

predominantly from the NE and SW and alluvial fans prograded from the basin-margin fault escarpments, represented by the deposits of the Derindere Member (Fig. 6a). These Upper Miocene alluvial-fan deposits show an overall upward fining trend, but thicken and coarsen towards the now faulted basin margins, represented by the Bozdağ and Dirmil Faults to the NW and SE of the basin, respectively. Locally, the alluvial-fan deposits rest in small patches on

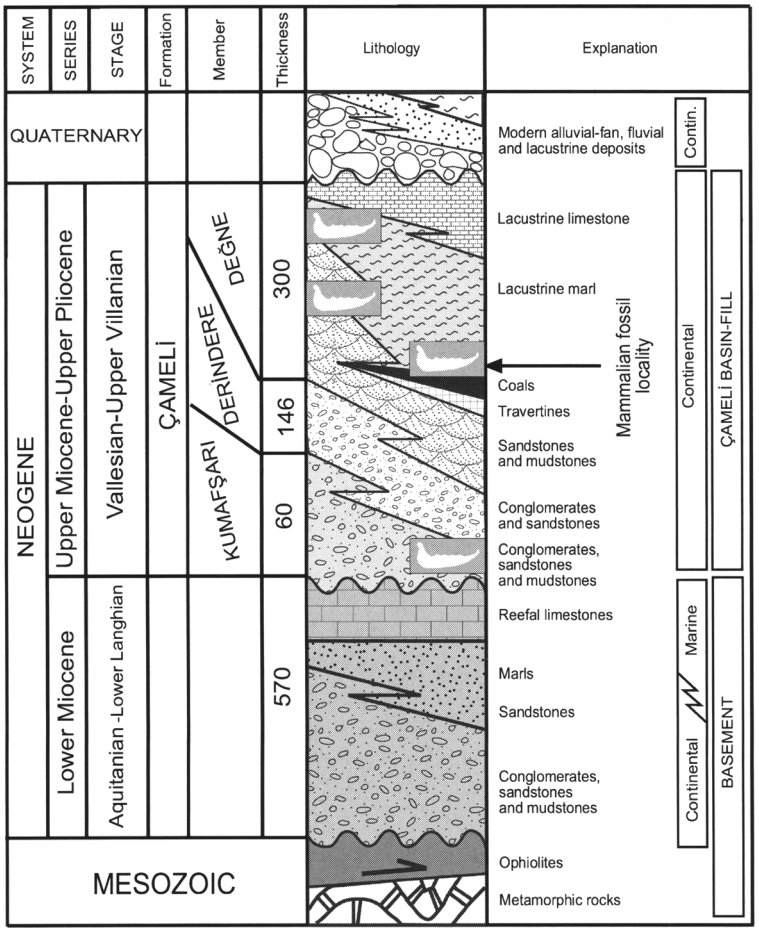

Fig. 4. Simplified statigraphy of the Çameli Basin (not to scale). Jaw symbols refer to levels with abundant mammal fossils.

the footwall block west of the Bozdağ Fault. A wedge shape of the stage 1 alluvial fans is particularly well seen at the western basin margin, but is obscured along the southeastern margin where later, ESE tilting has caused the burial of these deposits. Along the southwestern and northeastern basin margins, the Çameli Formation unconformably overlies the basement and locally Lower Miocene deposits (Fig. 3). All stage 1 deposits are characterized by dense, outcrop-scale growth faults (Fig. 7a), expressing synsedimentary extension throughout the Late Miocene.

Interpretation. The thickening of alluvial fan deposits towards the Bozdağ and Dirmil Faults suggests that these faults formed the basin margins by Late Miocene times. Because the depth to the base of the basin-fill succession is unknown directly adjacent to the basin-margin faults, we can only speculate about the amount of basin subsidence on either side of the basin. The general eastward tilt of the basin floor and asymmetrical distribution of sedimentary facies that is evident for subsequent stages of basin evolution cannot be affirmed for this stage. The presence of alluvial deposits on the footwall of the Bozdağ Fault indicates the potential of the alluvial fans to backlap across the basin margin, possibly controlled by continued basin deepening. The overall upward fining of the alluvial succession supports this basin deepening during stage 1. Palaeontological dates at the base of stage 2 (3.8–3.2 Ma; see next section) provide an estimate of *c.* 5–8 Ma for the duration of stage 1. The maximum basin depth is *c.* 210 m, based on the thickness of the stage 1 succession, not corrected for compaction, or the limited palaeo-water depths of the ephemeral-lake environment. These values suggest slow

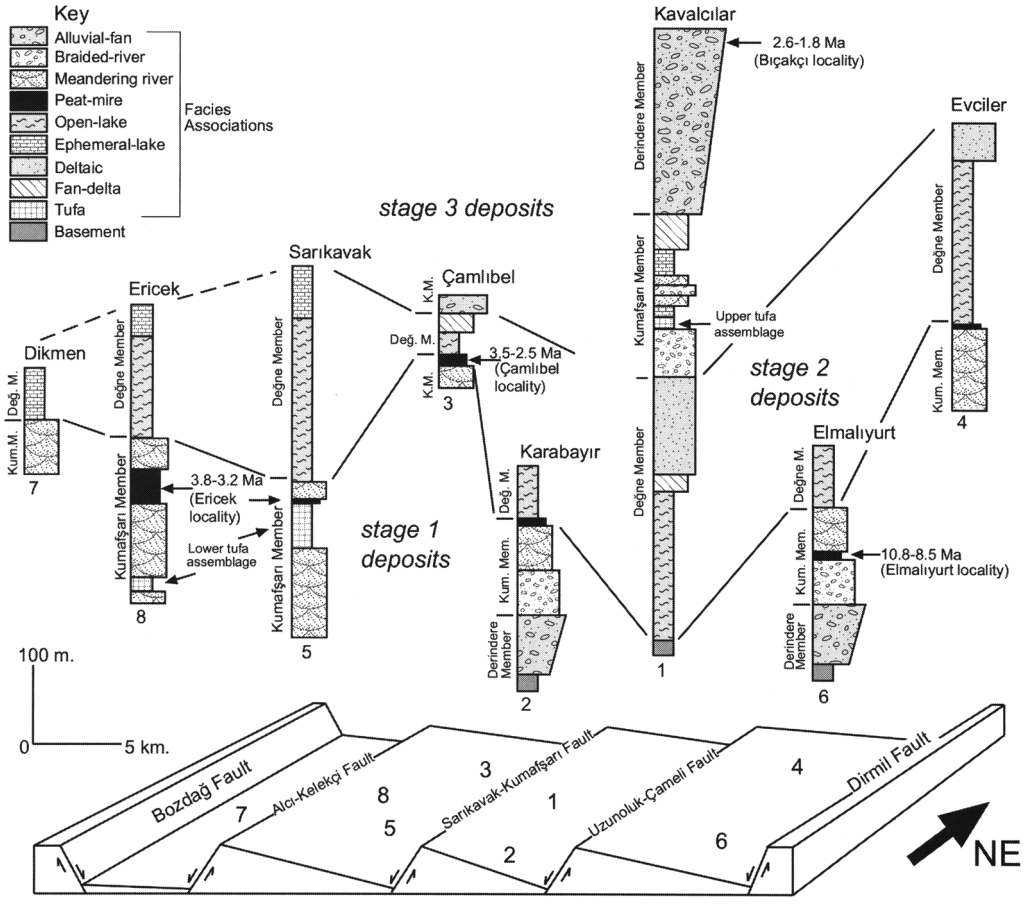

Fig. 5. Lateral correlation of measured logs in the Çameli Basin. (For location of logs see Figs 3 and 6.)

basin subsidence of the order of 3–4 cm ka^{-1}. However, erosion of sediment associated with block tilting during the later stages of basin development cannot be ruled out and could influence the basin subsidence rate.

Stage 2: intrabasinal faulting (Early–Mid-Pliocene transition)

Whereas the Late Miocene–Early Pliocene development of the Çameli Basin was characterized by slow overall subsidence, accommodated at the basin-margin faults, the following stage shows a distinctly different style as a result of the development of a NW-dipping normal fault in the centre of the graben. This Sarıkavak–Kumafşarı Fault Zone (SKFZ, Fig. 5) split the basin into two longitudinal compartments (Figs 3 and 6b). Close to the SKFZ, near Sarıkavak, the lowermost tufa unit has a thickness of 55 m, whereas at Ericek 5 km to west, a thickness of *c.*10 m is observed (Alçiçek & Özkul 2005), indicating a wedge shape of the tufa unit. Laterally (to the NW), the tufa interfingers with ephemeral-lake sediment and is overlain by fluvial and peat-mire sediments (Fig. 5). The latter sediments were sampled near Ericek and appear to abound in mammal micro- and macro-fossils. These include Rodentia teeth and bones, which indicate a Late Ruscinian (Zanclean–Piacenzian) age (3.8–3.2 Ma, Alçiçek *et al.* 2005). Also to the NE along the SKFZ, the tufa is transitional to the fluvial deposits of the Kumafşarı Member. Peat-mire deposits at the lateral transition between the fluvial Kumafşarı Member and the lacustrine Değne Member near Çamlıbel (Fig. 3) contain micro-remains of the mammal Rodentia, which indicate a Late Ruscinian–Early Villanian age (Piacenzian–Gelasian, 3.5–2.5 Ma, Alçiçek *et al.* 2005).

Table 1. *Lithofacies characteristics of the Çameli Formation in the Çameli Basin (based on Alçiçek 2001; Alçiçek* et al. *2004, 2005)*

Member	Facies associations	Lithology	Depositional environment
Değne (DMb)	Open-lake (OL)	Laminated marl Clayey limestone	Lacustrine
	Ephemeral-lake (EL)	Limestone Clayey limestone	
	Deltaic (D)	Massive–pebbly sandstone Stratified sandstone Planar cross-bedded sandstone Ripple cross-laminated sandstone	
	Fan-deltaic (FD)	Massive–pebbly sandstone Stratified sandstone Planar cross-stratified sandstone Clast-supported conglomerate Stratified conglomerate Laminated siltstone–mudstone	
Kumafşarı (KMb)	Tufa (T) (spring-outflow)	Travertine, micritic limestone Laminated siltstone–mudstone Laminated marl Clayey limestone	Fluvial
	Peat-mire (PM)	Coal Laminated siltstone–mudstone	
	Meandering-river (MR)	Planar cross-bedded sandstone Epsilon cross-bedded sandstone Stratified sandstone Laminated siltstone–mudstone Massive mudstone Ripple laminated sandstone Stratified conglomerate	
	Braided-river (BR)	Massive–pebbly sandstone Planar cross-bedded sandstone Clast-supported conglomerate	
Derindere (DrMb)	Alluvial-fan (AF)	Matrix-supported conglomerate Clast-supported conglomerate Stratified conglomerate Massive–pebbly sandstone Massive mudstone	Alluvial

Basinwide, the fluvial and peat-mire deposits are overlain by up to 220 m of monotonous open-lake deposits with local indications of wave reworking. In the Kavalcılar area (Fig. 3), the open-lake deposits directly overlie the basement ridge that was elevated in the footwall of the SKFZ (Fig. 7c). The relatively thick open-lake succession passes upwards into ephemeral-lake deposits in the basin centre. Towards the SW and NE, this facies passes into Gilbert-type river deltas, whereas near the basin-margin faults the lake deposits pass into Gilbert-type fan deltas (Fig. 6c). These deltas are characterized by steep foresets with abundant slump structures. Based on the irregular occurrence of these delta deposits, it is inferred that individual delta bodies have limited aerial extent.

Interpretation. The wedge shape of the tufa unit close to the SKFZ suggests a gradual, progressive tilt of the basin floor accommodated by fault displacement along the SKFZ. This caused a southeastward tilting of the basin floor and older (stage 1) basin deposits. The wedge shape implies a basin floor tilt of less than 1° during the tufa deposition, which explains why the contact with the overlying deposits shows no recognizable angular unconformity. The tufa is interpreted to originate from spring waters along the newly created intrabasinal SKFZ from which calcium carbonate was precipitated in the confined area of the local fault segment (see Guo & Riding 1998). Tufa or travertine (hotspring) deposits are generally recognized to be related to faults (Heimann & Sass 1989), especially in extensional tectonic settings (Altunel & Hancock 1993; Özkul *et al.* 2002). The general eastward dip of the basin floor and deepening towards the SKFZ is further interpreted from lateral facies transitions as

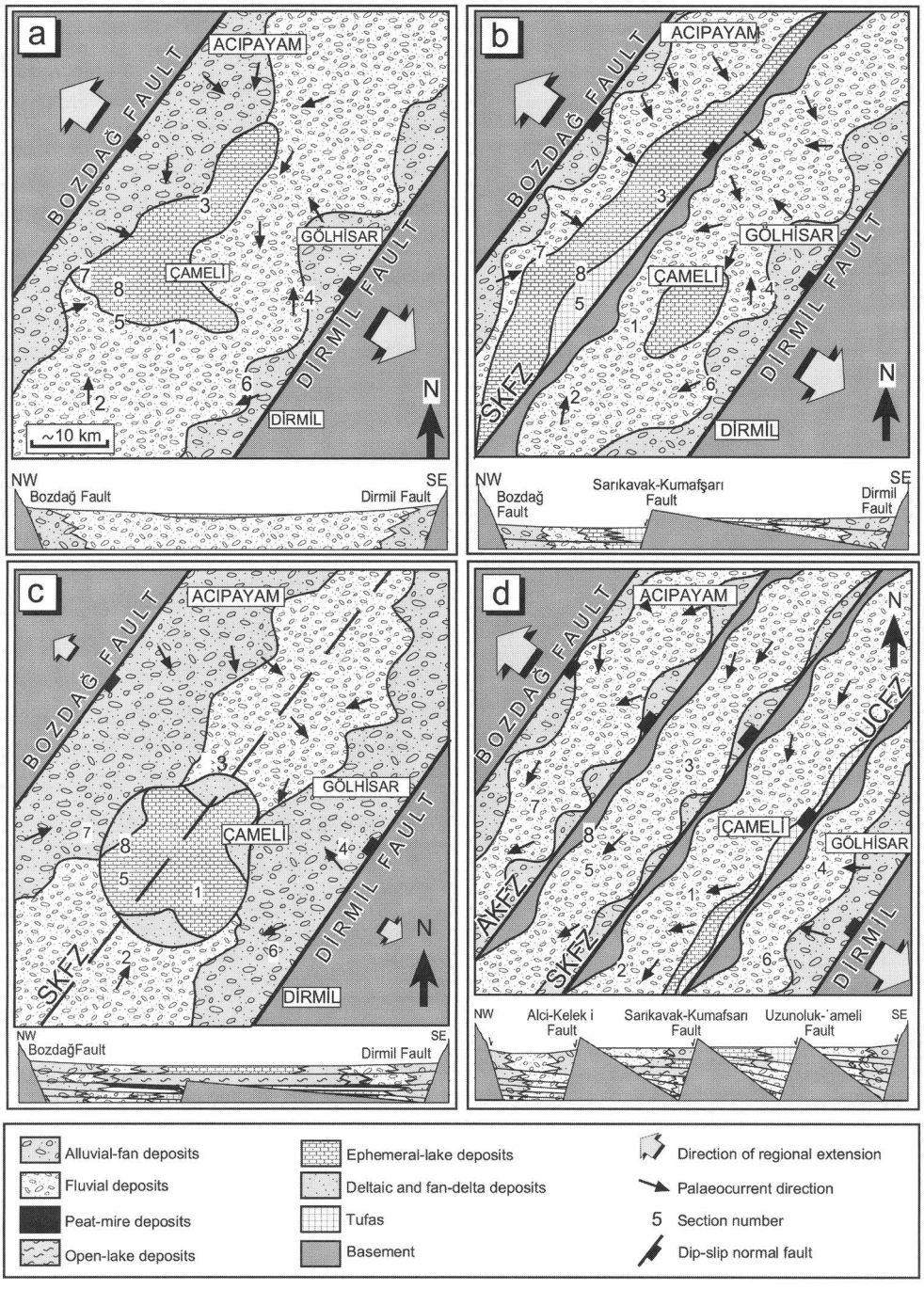

Fig. 6. Palaeogeographical reconstructions of successive stages of basin evolution in both map and cross-sectional view. (**a**) Opening of the basin during Late Miocene stage 1. (**b**) Development of intrabasinal Sarıkavak–Kumafşarı Fault Zone (SKFZ) and fault-related tufa wedge during the Early–Mid-Pliocene stage 2. (**c**) After overall deepening of the basin and basinwide occurrence of open-lake facies during the continuation of stage 2. The closure of stage 2 is marked by the re-occurrence of coarse clastic sedimentation. (**d**) Renewed intrabasinal faulting through the development of the Alcı–Kelekçi (AKFZ) and Uzunoluk–Çameli (UÇFZ) faults zones during the Late Pliocene.

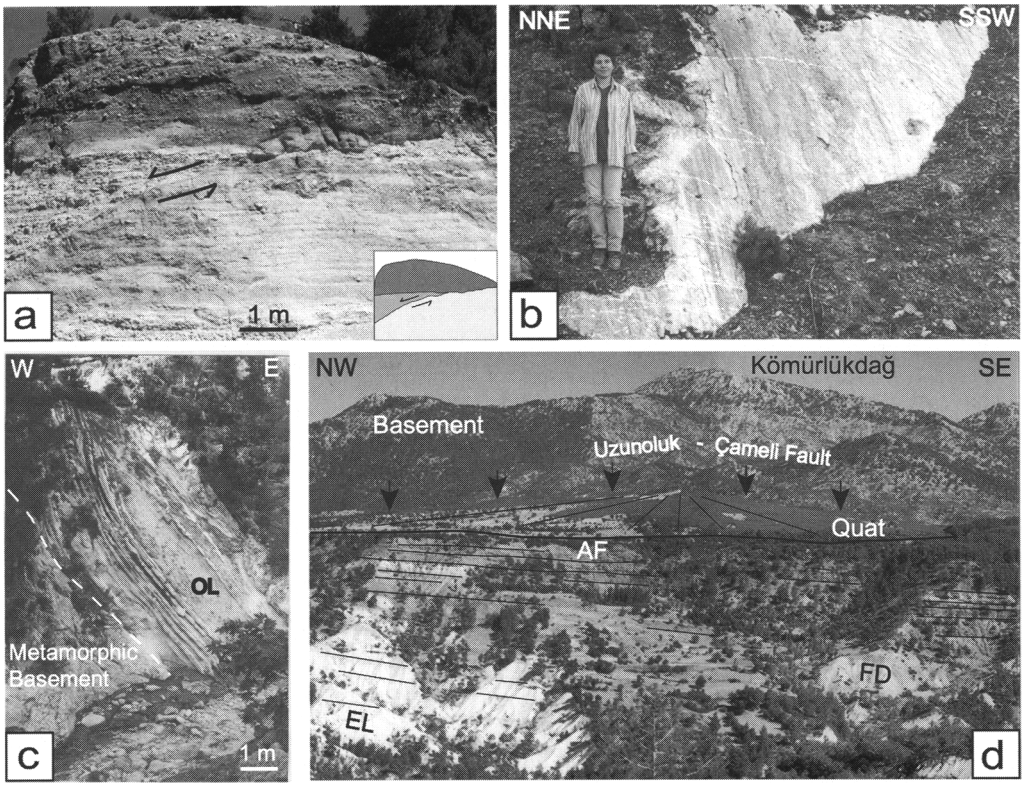

Fig. 7. Structural features related to the development of the Çameli Basin. (**a**) Growth fault associated with the stage 1 basin opening. (**b**) Fault plane of Uzunoluk–Çameli Fault with groove marks indicative of dip-slip normal faulting. (**c**) Down-section, to the east of (**d**), steeply tilted open-lake deposits (OL) overlie metamorphic basement rocks that were uplifted along the Sarıkavak–Kumafşarı Fault. The open-lake deposits correspond to the lowermost part of the Kavalcılar log in Fig. 5. (**d**) Typical eastward-tilted basin fill in the hanging-wall block of the Uzunoluk–Çameli fault (arrows+) SE of Bıçakçı (Fig. 3), corresponding to the ephemeral-lake (EL)–fan-delta (FD)–alluvial fan (AF) transition in the upper part of the Kavalcılar log in Figure 5. Bedding planes show faint indications of up-section decrease in dip angle as a result of syndepositional basin-floor tilting. Quat, Quaternary alluvial fan.

depicted in Figure 6b. Subtle increases in base level, accommodated by displacement along the SKFZ, may have caused inundation of the alluvial floodplains by the expanding lake, which locally led to peat-mire development. The deepening into deep-lake conditions and the complete submergence of the SKFZ intrabasinal ridge substantiates the continuation of basin-floor subsidence. Although the deep-lake deposits locally overlie the Dirmil and Bozdağ faults, there is no evidence that the lake extended far beyond these faults. Therefore, subsidence along the primary basin-margin faults is held responsible for the basin deepening.

The renewed input of coarse clastic material into the basin indicates either that basin subsidence slowed near the end of stage 2, or that sediment supply drastically increased. From the steep foresets with abundant slump structures and the limited aerial extent of the fluvial topset beds we deduce that only limited progradation of the fan deltas toward the deep lake occurred initially (see Postma 1990). Therefore, the shallowing in the basin centre towards ephemeral-lake conditions is not likely to be much influenced by an increased sediment input, but rather by slowing of basin subsidence. However, slowing of basin floor subsidence in combination with continued input of coarse-clastic sediment could have forced fan deltas to prograde towards the basin centre, as deduced from the upward transition of open-lake to ephemeral-lake and to deltaic deposits (Fig. 6).

Stage 3: renewed intrabasinal faulting (latest Pliocene)

After shallowing of the lake (Fig. 6c), a new phase of basin differentiation is represented by the generation of the Alcı–Kelekçi (AKFZ) and Uzunoluk–Çameli (UÇFZ) fault zones (Fig. 3). These faults caused the basin to be divided into narrower half-graben compartments (Fig. 6d) and are best recognizable where they cut the stage 2 open-lake sedimentary succession. The strikes and northwesterly dips of these new faults are similar to those of the pre-existing SKFZ. South of Çameli along the UÇFZ (Fig. 6d) the upper tufa unit exhibits a wedge shape with a thickness of 6 m near Kavalcılar (Fig. 5; Kavalcılar log) that rapidly increases towards the fault and is overlain by fluvial and alluvial-fan deposits.

Along the AKFZ, south of Kelekçi, a thick fan-delta sequence progrades westwards. Basinwards, the delta foresets are transitional to ephemeral-lake deposits, which are considered as delta front or prodelta equivalents of the fan delta. The fan-delta sequence is cut by a series of west-dipping normal faults that represent fault-parallel splays of the AKFZ (Fig. 3). One of these faults delimits an eastward–thickening 'upper' tufa wedge that includes intercalated slump deposits. This third stage of basin development occurred in Late Villanian time (Gelasian, 2.6–1.8 Ma, Alçiçek *et al.* 2005), as indicated by the remains of Rodentia fossils in the lower or distal part of alluvial-fan deposits that prograded onto the tufa deposits (Fig. 5). Towards the end of the Villanian (Late Gelasian) stage, the Çameli Basin was predominantly filled by fluvial and alluvial-fan depositional systems. Deep-lake conditions have not returned since that time. After the late Gelasian, basin-floor tilting continued, as inferred from the angular unconformity between the tilted stage 3 fluvial succession and the subhorizontal Pleistocene alluvium. Many north–south-trending outcrop-scale normal faults that cut and displace the stage 3 sediments are not present in the Pleistocene cover (Fig. 8a).

Interpretation. The stage 3 faulting episode caused further syndepositional southeastward tilting of the segmented basin-fill succession and its onset was accompanied by the deposition of the upper tufa unit. Our observations strongly suggest that eastward basin-floor tilting ceased at some ill-defined time during the Pliocene–Quaternary transition. In addition, the fact that deep-lake conditions did not return after the Villanian suggests an important lowering of the local base level at the Pliocene–Quaternary transition. In this scenario, the contemporaneous local base-level lowering can be explained by the cessation of basin-floor subsidence and by far more important Plio-Quaternary isostacy-driven regional surface uplift (see Westaway *et al.* 2003).

Stage 4: Quaternary

During the subsequent phase of Quaternary sedimentation several rivers incised the older basin fill and small alluvial fans developed at the dormant fault escarpments, which largely smoothed out the pre-existing tilted-block relief of the basin. Older Quaternary (?Pleistocene) river terrace deposits near Evciler unconformably overlie the tilted Neogene basin fill (Fig. 8a) and are, in turn, incised by more recent Quaternary fluvial systems that parallel the older basin axis. Along the southeastern basin margin, near Dirmil, an alluvial fan sequence is found that truncates the older lacustrine marls (Fig. 3). Close to the margin, this sequence consists of chaotic conglomerates with angular clasts representing scree and debris-flow deposits. To the west these chaotic deposits gradually pass into red and green clays rich in ostracodes and plant remains. Along the western basin margin, large scree sheets cover the Bozdağ Fault (Fig. 3). All of the Quaternary fluvial and alluvial deposits display subhorizontal bedding and are relatively poor in intraformational faults compared with the older deposits of the Çameli Basin.

The 020°-trending Cibyra Fault Zone (CbFZ) is, however, one of the few faults that indicates post-Pliocene fault activity in the Çameli Basin. This fault zone is characterized by numerous anastomosing subvertical fault splays. These show vertical offsets ranging from 0 to 50 cm, although some offsets of several metres were observed. The fault cuts a pre-existing basement contact of onlapping Pliocene (stage 3) fluvial deposits west of Gölhisar (fault locality b in Fig. 3). Consequently, the fault either juxtaposes peridotite basement and Neogene conglomerates, or cuts only the latter unit. The ancient city of Cibyra was built on the Pliocene clastic sedimentary rocks and its damaged stadium is located at the trace of one of the fault segments of the CbFZ (Fig. 3). According to Akyüz & Altunel (2001), the seating rows of the stadium were displaced sinistrally where they are crossed by the fault. There is ample archaeoseismolgical evidence that the stadium suffered serious earthquake damage (Fig. 8b), including a domino-style arrangement of fallen column blocks, the rotation and dilation of seating row blocks, and the almost complete collapse of the eastern side of the stadium. Akyüz & Altunel (2001) observed slickenside lineations on exposed fault surfaces to the south and north

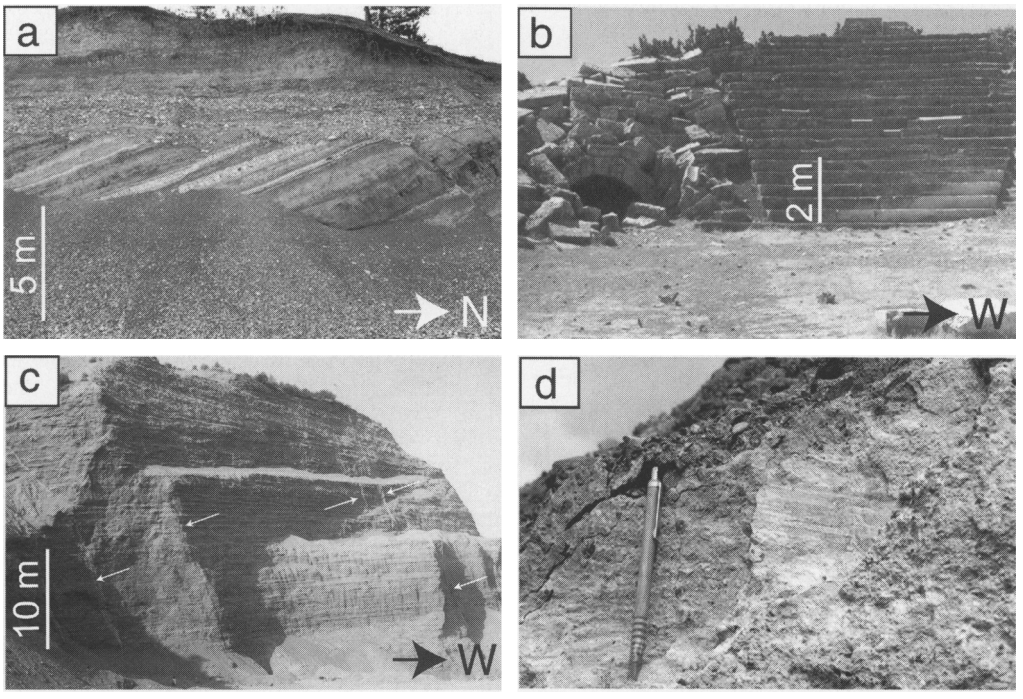

Fig. 8. Photographs showing characteristics of Quaternary strike-slip faulting: (**a**) older Quaternary (?Pleistocene) river terrace deposits unconformably overlie the tilted and faulted Neogene basin fill; (**b**) disturbed seating rows of the stadium at Cibyra; view to the south; (**c**) calcrete-filled, steep faults (see arrows) cutting tilted Pliocene conglomerates in the Kumkısığı quarry (see Fig. 3 for location); (**d**) detail of (**c**), showing near-horizontal slickensides indicative of dextral strike-slip motion on the fault plane.

of the stadium, which indicate sinistral oblique displacement of the CbFZ. We reinvestigated these localities and based on our fault kinematic data it appears that the fault zone comprises many differently oriented splays that exhibit either dextral, sinistral or normal displacement. The northernmost extent of the CbFZ is found in the Kumkısığı quarry (Fig. 3), where it cuts southeasterly tilted Pliocene conglomerates (Fig. 8c and d). There are also numerous faults with different orientations and with different styles of displacement, suggesting a complex deformation history. The analysis of these data is discussed in the next section.

Interpretation. Despite the base-level lowering at the Pliocene–Quaternary transition, during the Quaternary the basin was still fed by alluvial systems at both margins. The fact that these systems also cover the basin-margin faults suggests that fault displacement had ceased by Quaternary times. Active faults, such as the CbFZ, show negligible vertical offsets and we suppose that the thickness distribution of the Quaternary fan systems was not controlled by these faults. Rather, the pre-existing basin was filled by these young alluvial systems. The archaeoseismological evidence at Cibyra and the lithostratigraphic units affected limit the age of fault activity to post-Pliocene to subrecent, (i.e. the Quaternary). This young age is in accordance with the relatively small fault offsets.

Structural analysis

Fault measurements were made at several sites throughout the Çameli Basin (Fig. 3). Generally, the master faults cut through basement limestone and display slickensides, striae, or groove marks (tails and scratches produced by asperity ploughing). Smaller-scale faults that cut the clastic or lacustrine basin fill exhibit only striated surfaces. In a single case, a fractured and displaced clast could be used to determine the sense of slip. The estimated age of fault activity in most cases is based on fault-controlled sedimentological events (see previous section). Alternatively, the maximum age of fault activity is indicated by the age of the youngest affected stratigraphic unit. A

combination of both provides a time frame for fault activity during the last part of this period. In this study, fault data provide kinematic support for our model of basin evolution. The number of useful fault data are limited by available age constraints. Only 77 fault-kinematic indicators have therefore been considered for stress inversion, to obtain the orientations of the principal stress axes (see Table 2). Fault-slip analysis was performed with FaultkinWin 1.1 (a computer program for analysis of fault slip data by R. A. Almendinger *et al.* 2004).

Faults that are suggested to be active during stages 1–3 of the basin evolution have north–south to NE–SW orientations and exhibit kinematic evidence indicative of normal to normal–oblique-slip faults (Fig. 8a–c). A few NW–SE trending faults represent dextral oblique-slip faults that developed at the same time as the normal faults. Fault-plane solutions, often used as a first approximation of the stresses (Marrett & Almendinger, 1990), indicate that this fault pattern was produced under NW–SE extension (Fig. 9a–c).

Fault data for stage 4 of the basin evolution collected in the complex Cibyra Fault Zone and the Evciler area show many kinematic inconsistencies. This is demonstrated by the P/T scatter plot (Fig. 9g), which shows overlaps between the orientations of P and T axes of individual faults. Such overlap between P and T axes is often produced by a combination of fault kinematic indicators that were generated under different stress regimes. Representing the fault data in one single fault-plane solution gives an incorrect result that does not account for the stresses exerted by individual tectonic regimes. To overcome this problem we sorted the fault data according to the orientations of the P and T axes to produce kinematically compatible groups of fault data. Performing this exercise on the Cibyra and Evciler fault sets produces two groups of compatible fault data, which are referred to as stage 4a and stage 4b (Fig. 9). The first set is represented by normal and normal–oblique faults with north–south to NE–SW orientations in combination with a few north–south-trending sinistral strike-slip faults (Fig. 9d). The fault-plane solutions of these fault sets suggest that the faults were produced under NW–SE extension, and are thus kinematically comparable with the stage 1–3 faults. The second subset of faults dominantly consists of NE–SW-trending dextral strike-slip faults and NW–SE-trending normal faults (Fig. 9e). At both the Cibyra and Evciler sites, a few NNW–SSE-trending sinistral strike-slip faults occur as well. Fault-plane solutions for both sites (Fig. 9e), show the different orientation of the T axes and the near-horizontal plunge of the P axes compared with the stage 1–4a faults, suggesting that this fault set was produced in a strike-slip tectonic regime.

In conclusion, two sets of fault-kinematic data are recognized that relate to different types of deformation and that were probably generated under different tectonic regimes. The translation from observed deformation to stresses exerted by regional tectonic processes is facilitated by stress inversion techniques. Following the method described by Marrett & Almendinger (1990), the orientations of stress axes are based on Bingham distribution statistics providing directional maxima of the shortening and extension axes of a fault array. The stress tensor aspect ratio Φ defined as $\sigma_2-\sigma_3/\sigma_1-\sigma_3$, was determined to indicate the tectonic regime.

A best-fit stress inversion for the stage 1–4a faults yields a horizontal σ_3 oriented towards 311° and a vertical maximum compression σ_1. In combination with the stress axes, the stress-ellipsoid shape parameter $\Phi=0.65$ indicates plane stress under NW–SE extension (D_1 in Fig. 9f). Stress inversion for the stage 4b faults shows a slightly inclined σ_3 plunging toward 195° and a σ_1 axis moderately inclined toward 088°. With $\Phi=0.32$, the orientations of the inclined stress axes indicate deformation in transtension (D_2 in Fig. 9g). This transtensional regime is resolved by dextral shear along NE–SW-trending synthetic strike-slip faults, sinistral shear along NNW–SSE-trending antithetic strike-slip faults and tension at NW–SE-trending normal faults.

The onset of D_1 extension is well constrained by the Late Miocene initiation of the Çameli Basin. Continued extension caused segmentation of the tilted basin floor, resulting in local uplift or deepening that characterizes the Late Miocene–Late Pliocene sedimentation patterns of the basin. Although no tectonosedimentary evidence was found, the D_1 extension obviously continued into the early Quaternary (stage 4a), as is evidenced by fault data from the Cibyra and Evciler localities. The transtensional D_2 deformation does not clearly overprint the former D_1 faults, but the late Quaternary (Holocene) timing is well constrained by the historical ruptures that destroyed Cibyra's stadium. However, we did not find that the recent colluvium was affected by these D_2 faults.

Discussion

The present study of the Çameli Basin, involving basin analysis, and structural analysis, provides the first detailed time–stratigraphic framework

Table 2. *Fault-slip data collected in the study area providing the basis for kinematic interpretations (stress inversion) presented in Figure 9*

Site	Fault	Fault strike (RHR)	Fault dip	Rake (0–180°)	Indicator type	Upper block	Lower block
a	CbFZ	024	83	158	str.	KMb	KMb
		004	90	180	str.	KMb	KMb
b	CbFZ	240	74	174	str.	KMb	KMb
		230	75	30	str.	KMb	KMb
		224	86	160	str.	KMb	KMb
		226	63	120	str.	KMb	KMb
		227	68	108	str.	KMb	KMb
		225	71	70	o.c.	KMb	KMb
		170	70	90	o.c.	KMb	KMb
		046	73	95	s.s.	KMb	KMb
		272	58	0	str.	KMb	KMb
		246	58	75	s.s.	KMb	KMb
		249	81	50	str.	KMb	KMb
		224	78	70	g.m.	KMb	KMb
		200	58	75	g.m.	KMb	KMb
		116	70	110	s.s.	KMb	KMb
		180	65	80	g.m.	KMb	KMb
		235	61	155	str.	KMb	KMb
		122	41	90	str.	KMb	KMb
		247	83	150	str.	KMb	KMb
		260	80	165	str.	KMb	KMb
		232	75	150	str.	KMb	KMb
		261	81	53	str.	KMb	KMb
		123	78	88	str.	KMb	KMb
		231	73	160	str.	KMb	KMb
		060	68	110	str.	KMb	KMb
		180	80	135	str.	KMb	KMb
c	N of Evciler	160	65	150	str.	KMb	KMb
		175	64	123	str.	KMb	KMb
		150	48	165	str.	KMb	KMb
		208	87	80	str.	KMb	KMb
		330	85	100	str.	KMb	KMb
		355	89	105	str.	KMb	KMb
		002	89	90	str.	KMb	KMb
d	Yaprakh dam	353	73	80	g.m.	DMb	DMb
		012	84	120	g.m.	DMb	DMb
		018	70	68	g.m.	DMb	DMb
		002	87	100	g.m.	DMb	DMb
		192	60	80	g.m.	DMb	DMb
e	UÇFZ	189	54	88	g.m.	Basm	DrMb
		193	52	127	str.	Basm	DrMb
		200	48	120	str.	Basm	DrMb
		194	50	90	g.m.	Basm	DrMb
		178	41	108	s.s.	Basm	DrMb
		170	42	115	str.	Basm	DrMb
		237	54	170	str.	Basm	Basm
		229	40	180	str.	Basm	Basm
		223	40	125	s.s.	Basm	DrMb
		253	51	180	str.	Basm	DrMb
f	SKFZ	226	52	90	str.	Basm	DMb
		045	42	90	str.	Basm	Basm
g	SKFZ	038	68	100	g.m.	DMb	KMb
		065	65	70	g.m.	DMb	KMb
		270	65	90	g.m.	Basm	Basm
		255	53	90	g.m.	Basm	Basm
		234	64	72	g.m.	Basm	Basm
		229	43	95	g.m.	Basm	Basm
		054	40	63	str.	DMb	DMb
		230	29	90	str.	DMb	DMb

Table 2. *Continued*

Site	Fault	Fault strike (RHR)	Fault dip	Rake (0–180°)	Indicator type	Upper block	Lower block
h	CbFZ	228	88	90	str.	KMb	KMb
		350	80	55	str.	KMb	KMb
		035	87	105	str.	KMb	KMb
		000	90	30	str.	KMb	KMb
i	SKFZ	181	79	100	s.s.	Basm	Basm
		178	71	95	s.s.	Basm	Basm
		204	64	110	g.m.	Basm	Basm
j	AKFZ	200	52	70	s.s.	KMb	KMb
		060	71	45	g.m.	KMb	KMb
k	AKFZ	235	73	85	g.m.	DMb	DMb
		222	42	95		DMb	DMb
l	BFZ	021	60	100	str.	LMio	DrMb
		010	70	110	g.m.	LMio	LMio
		135	83	120	s.s.	LMio	LMio
		220	34	108	s.s.	LMio	LMio
		090	65	105	s.s.	LMio	LMio
		020	43	90	g.m.	LMio	LMio
		020	77	100	s.s.	LMio	LMio

Localities (a–l) are indicated in Figure 3. Fault strikes according to right-hand rule (RHR). Rakes of kinematic indicators range form 0° (pure sinistral slip), through 90° (pure dip slip) to 180° (pure dextral slip). Type of kinematic indicator: str., striae; g.m., groove mark; o.c., offset clast(s); s.s., slickensides. Lithologies: Basm, basement; DMb, Değne Member; KMb, Kumafşarı Member; DrMb, Derindere Member; LMio, Lower Miocene deposits (basement); CbFZ, Cibyra Fault Zone; UÇFZ, Uzunoluk–Çameli Fault Zone; SKFZ, Sarıkavak–Çameli Fault Zone; AKFZ, Alcı–Kelekçi Fault Zone; BFZ, Bozdağ Fault Zone.

for the neotectonic development of Neogene grabens in the Fethiye Burdur Fault Zone. However, it is not exactly clear what are the tectonic driving forces that trigger the formation of these basins. Collins & Robertson (1998, 1999) documented the southeastward emplacement of the Lycian allochthon during three episodes starting in the Late Cretaceous. The final emplacement over the most proximal foredeep (Kaş Basin; Fig. 1) occurred in Late Miocene (Tortonian) time. Biostratigraphic evidence presented here indicates that sedimentation in the Çameli Basin had commenced by Vallesian time (Early Tortonian; 10.8–8.5 Ma), suggesting that the extensional basin opening coincided with this final phase of thrusting. Extension thus occurred in the hinterland zone of the emplacing nappes and coeval contraction occurred in the Lycian foreland zone (Kaş Basin). Closer to the nappe front, i.e. to the SE, this extension probably did not develop during the Late Miocene. This is exemplified by the fact that the Eşen Çay Basin (Fig. 1) originated as a NE–SW-trending fluviolacustrine basin in a ramp-fold close to the Lycian thrust front (ten Veen 2004). Here, NW–SE extension is reported only for the Late Pliocene–Pleistocene period. Such a combination of extension in the hinterland coeval with contraction in the foreland is interpreted to result from 'orogenic collapse' (Seyitoğlu *et al.* 1996; Collins & Robertson 1999, and references therein). The structural style of the NE–SW grabens in southwestern Anatolia was thus possibly established during the final stage of nappe emplacement, which also explains the parallelism of the Lycian thrust front and extensional basins. Price & Scott (1991) also mentioned the presence of a NE–SW-trending fabric within the pre-Neogene basement of the Burdur region, which might have influenced the orientation of faults formed during the subsequent Neogene and Quaternary extension. The Pliocene–Quaternary westward escape of Anatolia, which generated north–south extension in the EAEP (Purvis & Robertson 2004), thus postdates the foundering of NE–SW-trending basins in the FBFZ. However, westward escape of Anatolia can be still considered as one of the possible driving mechanism for extension in SW Anatolia during the younger, Pliocene–Quaternary period of extension.

Based on fault kinematic data for basin-bounding faults of the Quaternary Burdur, Acıgöl and Çivril basins, Price & Scott (1994) identified NW–SE-directed extension. Kinematic data of numerous mesoscale faults that cut the Late Miocene–Late Pliocene Çameli basin fill reveal similar orientations of palaeostress axes. The earthquake source mechanisms of the

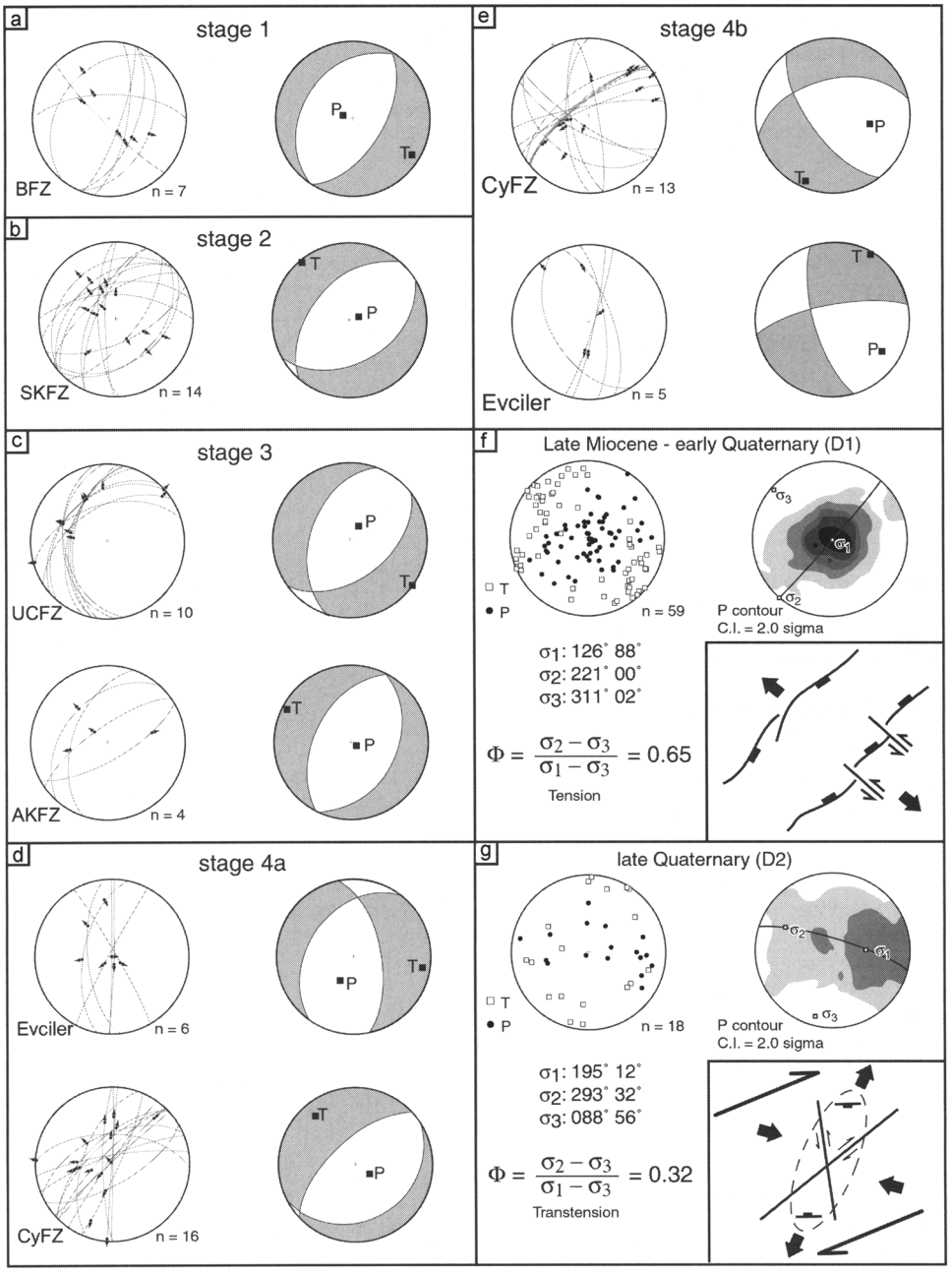

Fig. 9. (**a**–**e**) Fault data for the Çameli faults on lower hemisphere equal area projections together with fault-plane solutions used as a first approximation of the stress field (see text for explanation). (**f**) Stress inversion results of Late Miocene–early Quaternary (D_1) deformation, characterized by NW–SE extension with $\sigma_1 > \sigma_2 > \sigma_3$ and σ_3 horizontal. (**g**) Stress inversion results of late Quaternary (D_2) deformation, characterized by inclinations of all stress axes, which in this case is indicative of a dextral-transtensional tectonics regime, resolved by dextral shear along NE–SW-trending synthetic strike-slip faults, sinistral shear along NNW–SSE-trending antithetic strike-slip faults and tension at NW–SE-trending normal faults.

May 12 1971 Burdur earthquake sequence also confirm the NW–SE orientation of extension (Taymaz & Price 1992). Price & Scott (1994) suggested that the discrepancy between north–south extension in Western Anatolia and the NW–SE extension could be explained in terms of differences in crustal thickness between the rapidly extending Aegean region and the stable unstretched central Anatolia plateau to the east. Block rotations about vertical axes are accommodated by a hypothetical north–south dextral shear zone, which accounts for NE–SW faults with sinistral-normal senses of slip. This concept is somewhat outdated, because of the underestimated role of the major NW–SE-trending Dinar Fault. The 1 October 1995 Dinar earthquake, with a 10 km long surface rupture indicating normal faulting under NE–SW extension, changed existing ideas concerning the regional tectonic setting. Temiz *et al.* (1997) reintroduced the preliminary cross-fault model of Westaway (1990) for the Burdur–Dinar area and proposed a two-stage evolution. The first stage of NE–SW extension caused initiation of the south-facing Dinar breakaway fault and led to the formation of the Burdur, Acıgöl and Çivril 'hanging-wall' area. Temiz *et al.* claimed that at this stage sinistral oblique slip along the Burdur and Acıgöl faults accommodated differential stretching of the hanging wall. During the second stage, extension occurred in both NE–SW (Dinar Fault) and NW–SE (Burdur, Acıgöl and Çivril faults) directions.

The east–west to WNW–ESE extension of the Eşen Çay Basin, forming the southernmost basin in the FBFZ of southwestern Turkey, is suggested to be related to the kinematic effects of outward growth of the Hellenic forearc (ten Veen 2004). The present-day GPS velocity field adequately demonstrates this east–west extension (e.g. McClusky *et al.* 2000) with effects that are also observed on Rhodes and Crete (ten Veen & Kleinspehn 2002, 2003) and possibly in the Isparta Angle, although interpreted differently by Glover & Robertson (1998). The GPS velocity field is thought to be determined by the westward extrusion of Anatolia in combination with effects of subduction rollback and back-arc extension. Ten Veen (2004) suggested that a time-transgressive addition of a sinistral shear component was produced by the northeastward propagating transcurrent motions of forearc slivers that sheared from the expanding forearc as continental collision with the African promontory started. This process began on Crete and Rhodes in the Late Pliocene and is as young as the Holocene in the Eşen Çay Basin. Based on these earlier finding and models, a geologically young (even historical) transtensional deformation in the Çameli Basin is thus expected. However, throughout the entire eastern Hellenic forearc, transtension was always combined with NE–SW extension and sinistral shear resolved on NE- to ENE-trending faults. The 'young' transtension in the Çameli basin is, instead, explained by a combination of NE–SW extension and dextral shear resolved on NE-trending faults.

The Çameli Basin area can, thus, be regarded as an interference zone of at least three different tectonic regimes: (1) outward growth of the eastern Hellenic forearc, resulting in NE–SW extension; (2) tectonic escape represented by strike-slip faulting approximately along the strike of the eastern forearc; (3) NE–SW extension towards the north of the FBFZ (Dinar and Denizli grabens), which can be interpreted as internal deformation related to Anatolian extrusion (Eyidoğan & Barka 1996). The development of a particular basin probably involves the effects of more than one regime, although one stress field might dominate in some cases or could prevail during a certain time period. The model presented in Figure 10 illustrates how the southern part of the FBFZ is influenced by the sinistral transcurrent motions along, and expansion, of the eastern Hellenic Arc (1 and 2), while at the same time the northern part is influenced by the north–south extrusion-related extension and Hellenic Arc expansion (3 and 1). The NW–SE-trending Çavdır Fault (Fig. 3), forming the northern limit of the Çameli Basin, might be another important fault breakaway fault on a smaller scale, comparable with the Dinar fault. Differential motion of its hanging-wall block could have induced the dextral motion at the Cibyra Fault Zone, which is supported by the fact the latter fault does not continue into the footwall block of the Çavdır Fault. Additionally, the increasing importance of NE–SW extension northward along the FBFZ is likely to limit the effect of sinistral transcurrent motions occurring in the southern part.

Although local strike-slip faults are present in the FBFZ, from south to north they are related to different tectonic processes. Thus, it appears that this feature is better described as a broad zone of isolated or interconnected NE–SW-trending basins that formed under prevailing NW–SE extension in combination with local tectonic regimes that produce(d) the strike-slip faulting.

Conclusions

(1) In the Late Miocene the Çameli Basin was established as a broad fault-bounded fluviolacustrine basin that experienced NW–SE extension in the northerly hinterland zone of the still emplacing Lycian nappes.

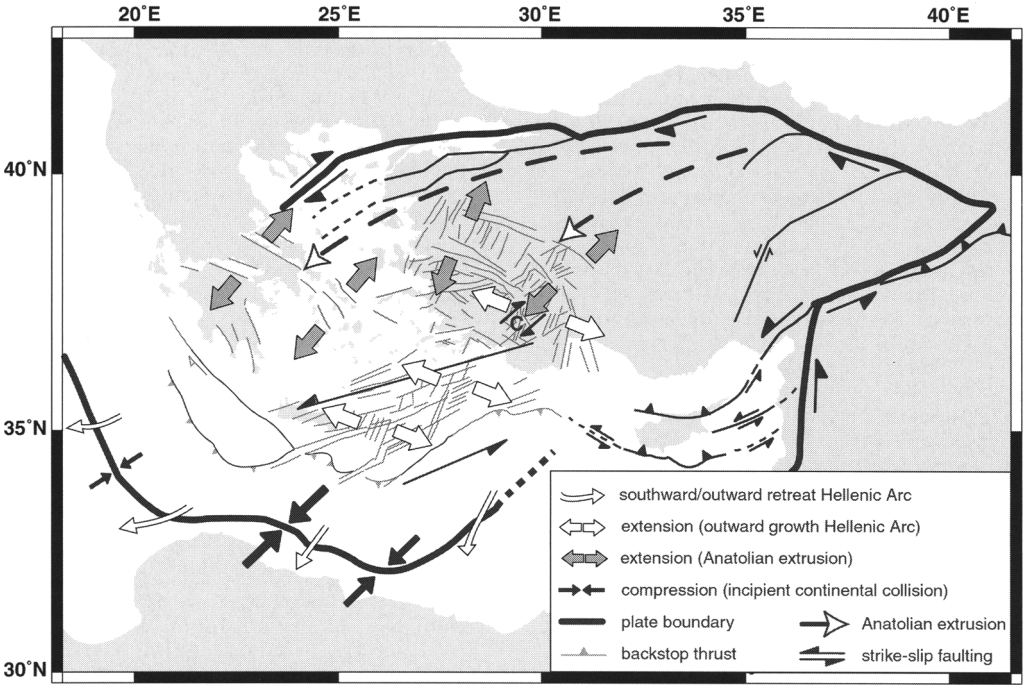

Fig. 10. Sketch diagram showing the inferred Holocene–Recent geodynamic mechanisms that contribute to the deformation of the Çameli Basin (indicated with bold C). Mechanisms include: (1) outward growth of the eastern Hellenic forearc, resulting in NE–SW extension; (2) tectonic escape represented by strike-slip faulting approximately along the strike of the eastern forearc; (3) NE–SW extension in central western Anatolia related to the Anatolian extrusion. Whereas sinistral strike-slip faulting penetrated only the southernmost part of Turkey, the dextral strike-slip faults in the Çameli Basin are interpreted to accommodate NW–SE extension on general NE–SW-trending faults.

(2) Outward growth of the Hellenic Arc, as a result of westward Anatolian escape, accompanied a Pliocene period of intensified NW–SE extension that resulted in the formation of several new intrabasinal fault zones. By the end of the Pliocene, these faults split the basin longitudinally into four narrow half-graben compartments.

(3) Holocene deformation is characterized by continued NW–SE extension and dextral shear resolved on NE–SW-trending strike-slip faults. Dextral strike-slip faulting is localized and accommodates the activity of NW–SE-trending normal faults.

(4) Sinistral strike-slip faulting, continuing along the eastern Hellenic Arc and penetrating the southernmost part of Turkey, has not yet reached the Çameli Basin area.

(5) The entire FBFZ is an expression of several regional tectonic processes including: (a) outward growth of the eastern Hellenic forearc, resulting in NE–SW extension; (b) tectonic escape represented by strike-slip faulting approximately along the strike of the eastern Hellenic forearc; (c) NE–SW extension towards the north of the FBFZ, related to westward Anatolian escape.

This study was supported by the Scientific and Technical Research Council of Turkey (TÜBİTAK) research grant YDABÇAG 100Y004 to M.C. Alçiçek and Dutch Science Foundation, NWO grant 831.48.009 to J.H.T.Veen. Some figures were created using the GMT (Generic Mapping Tools) software, and we are indebted to its authors P. Wessel and W. Smith for making it available. This manuscript benefited from constructive reviews by A. H. F. Robertson and S. J. Boulton.

References

AKYÜZ, H. S. & ALTUNEL, E. 2001. Geological and archaeological evidence for post-Roman earthquake surface faulting at Cibyra, SW Turkey. *Geodinamica Acta*, **14**, 95–101.

ALÇIÇEK, M. C. 2001. *Sedimentological investigation of Çameli Basin (Late Miocene–Late Pliocene,*

Denizli, SW Anatolia). PhD thesis, Ankara University.

ALÇIÇEK, M. C. & ÖZKUL, M. 2005. Extensional faulting induced tufa precipitation in the Neogene Çameli Basin of southwestern Anatolia, Turkey. *In*: ÖZKUL, M., YAĞIZ, S. & JONES, B. (eds) *Proceedings of the First International Symposium on Travertines and Technologies Exhibition, Proceedings, 21–25 September, Denizli, Turkey*, 120–127.

ALÇIÇEK, M. C., KAZANCI, N., ÇEMEN, İ. & ÖZKUL, M. 2002. Strike-slip faulting in the Çameli basin, southwestern Turkey: implications for inland transform prolongation of the Hellenic subduction zone. Annual Meeting of the Geological Society of America, 27–30 October 2002, Denver. *Abstracts with Programs*, **34**, 111–114, 250.

ALÇIÇEK, M. C., KAZANCI, N., ÖZKUL, M. & ŞEN, Ş. 2004. Sedimentary infill and geological evolution of the Çameli Basin, Denizli, SW Turkey. *Bulletin of Mineral Research and Exploration of Turkey*, **128**, 99–123.

ALÇIÇEK, M. C., KAZANCI, N. & ÖZKUL, M. 2005. Multiple rifting pulses and sedimentation pattern in the Çameli Basin, southwestern Anatolia, Turkey. *In*: KELLING, G., ROBERTSON, A. H. F. & VAN BUCHEM, F. H. P (eds), *Cenozoic Sedimentary Basins of South Central Turkey. Sedimentary Geology, Special Issue*, **173**(1–4), 409–431.

ALTINLI, I. E. 1955. The geology of southern Denizli. *Revue de la Faculté des Sciences de l'Université d'Istanbul, Série B: Sciences Naturelles*, **20**(1–2), 1–47.

ALTUNEL, E. & HANCOCK, P. L. 1993. Morphology and structural setting of Quaternary travertines at Pamukkale, Turkey. *Geological Journal*, **28**, 335–346.

BARKA, A., REILINGER, R., ŞAROĞLU, F. & ŞENGÖR, A. M. C. 1997. The Isparta Angle: its importance in the neotectonics of the Eastern Mediterranean region. *In*: PIŞKIN, Ö., ERGÜN, M., SAVAŞGIN, M. Y. & TARCAN, G. (eds) *International Earth Science Colloquium on the Aegean Region, 9–14 October 1995, Proceedings*, **1**, 3–17, Izmir, Turkey.

BECKER-PLATEN, J. D. 1970. *Lithostratigraphische Unterschungen im Kanozoikum Südwest Anatoliens (Türkei) (Kanozoikum und Braunkohlen der Turkei)*. Beihefte zum Geologischen Jahrbuch, **97**.

BOZKURT, E. 2001. Neotectonics of Turkey—a synthesis. *Geodinamica Acta*, **14**, 3–30.

BOZKURT, E. 2003. Origin of NE-trending basins in western Turkey. *Geodinamica Acta*, **16**, 61–81.

COLLINS, A. & ROBERTSON, A. H. F. 1998. Processes of Late Cretaceous to Late Miocene episodic thrust-sheet translations in the Lycian Taurides, SW Turkey. *Journal of the Geological Society, London*, **155**, 759–772.

COLLINS, A. & ROBERTSON, A. H. F. 1999. Evolution of the Lycian Allochthon, western Turkey, as a north-facing Late Palaeozoic to Mesozoic rift and passive continental margin. *Geological Journal*, **34**, 107–138.

COLLINS, A. & ROBERTSON, A. H. F. 2003. Kinematic evidence for Late Mesozoic–Miocene emplacement of the Lycian Allochthon over the Western Anatolide Belt, SW Turkey. *Geological Journal*, **38**, 295–310.

DE GRACIANSKY, P. C. 1972. *Récherches géologiques dans le Taurus Lycien Occidental*. DSc thesis, Université de Paris-Sud.

DUMONT, J. F., POISSON, A. & ŞAHINCI, A. 1979. Sur l'existence de coulissement sénestre récent a l'extrémité orientale de l'arc égéen (sud-ouest de la Turquie). *Comptes Rendus de l'Académie des Sciences*, **289**, 261–264.

ERAKMAN, B., MEŞHUR, M., GÜL, M. A., ALKAN, H., ÖZTAŞ, Y. & AKPINAR, M. 1982. *Toros projesine bağlı Kalkan–Köyceğiz–Çameli–Tefenni arasında kalan alanın jeolojisi ve hidrokarbon olanakları raporu*. Natural Oil and Natural Gas Company of Turkey (TPAO), Ankara, Technical Report, **1732**.

EYIDOĞAN, H. & BARKA, A. 1996. The 1 October 1995 Dinar earthquake, SW Turkey. *Terra Nova*, **8**, 479–485.

FLECKER, R., ROBERTSON, A. H. F., POISSON, A. & MÜLLER, C. 1995. Facies and tectonic significance of two contrasting Miocene basins in south coastal Turkey. *Terra Nova*, **7**, 221–232.

FLECKER, R., POISSON, A. & ROBERTSON, A. H. F. 2005. Facies and palaeogeographic evidence for the Miocene evolution of the Isparta Angle in its regional Eastern Mediterranean context. *In*: KELLING, G., ROBERTSON, A. H. F. & VAN BUCHEM, F. H. P. (eds) *Cenozoic Sedimentary Basins of South Central Turkey. Sedimentary Geology, Special Issue*, **173**(1–4), 277–314.

GLOVER, C. & ROBERTSON, A. H. F. 1998. Neotectonic intersection of the Aegean and Cyprus tectonic arcs: extensional and strike-slip faulting in the Isparta Angle, SW Turkey. *Tectonophysics*, **298**, 103–132.

GUO, L. & RIDING, R. 1998. Hot-spring travertine facies and sequences, Late Pleistocene Rapolano Terme, Italy. *Sedimentology*, **45**, 163–180.

HEIMANN, A. & SASS, E. 1989. Travertines in the northern Hula Valley, Israel. *Sedimentology*, **36**, 95–108.

KOÇYIĞIT, A., ÜNAY, E. & SARAÇ, G. 2000. Episodic graben formation and extensional neotectonic regime in west Central Anatolia and the Isparta Angle: a case study in the Akşehir–Afyon Graben, Turkey. *In*: BOZKURT, E., WINCHESTER, J. A. & PIPER, J. D. A. (eds) *Tectonics and Magmatism in Turkey and the Surrounding Area*. Geological Society, London, Special Publications, **173**, 405–421.

MARRETT, R. A. & ALMENDINGER, R. W. 1990. Kinematic analysis of fault-slip data. *Journal of Structural Geology*, **12**, 973–986.

MCCLUSKY, S., BALASSAANIAN, S., BARKA, A., *et al.* 2000. Global Positioning System constraints on plate kinematics and dynamics in the eastern Mediterranean and Caucusus. *Journal of Geophysical Research*, **105**(B3), 5695–5719.

MEŞHUR, M. & AKPINAR, M. 1984. *Yatağan–Milas–Bodrum–Karacasu–Kale–Acıpayam-Tavas civarlarının jeolojisi ve petrol olanakları*. Natural Oil and Natural Gas Company of Turkey (TPAO), Ankara, Technical Report, **1963**.

ÖZKUL, M., VAROL, B. & ALÇIÇEK, M. C. 2002. Depositional environments and petrography of Denizli travertines). *Bulletin of Mineral Research and Exploration of Turkey*, **125**, 13–29.

POSTMA, G. 1990. Depositional architecture and facies of river and fan deltas: a synthesis. *In*: COLELLA, A. & PRIOR, D. B. (eds) *Coarse Grained Deltas*. International Association of Sedimen to Logists. Special Publications, **10**, 13–27.

PRICE, S. P. & SCOTT, B. C. 1991. Pliocene Burdur basin, SW Turkey: tectonics, seismicity and sedimentation. *Journal of the Geological Society, London*, **148**, 345–354.

PRICE, S. P. & SCOTT, B. C. 1994. Fault-block rotations at the edge of a zone of continental extension, south-west Turkey. *Journal of Structural Geology*, **16**, 381–392.

PURVIS, M. & ROBERTSON, A. H. F. 2004. A pulsed extension model for the Neogene–Recent E–W-trending Alaşehir Graben and the NE–SW-trending Selendi and Gördes Basins, western Turkey. *In*: TAYMAZ, T., WESTAWAY, R. & REILINGER, R. (eds) *Active Faulting and Crustal Deformation in the Eastern Mediterranean Region. Tectonophysics*, **391**(1–4), 171–201.

PURVIS, M. & ROBERTSON, A. H. F. 2005*a*. Sedimentation of the Neogene–Recent Alaşehir (Gediz) continental graben system used to test alternative tectonic models for western (Aegean) Turkey. *In*: KELLING, G., ROBERTSON, A. H. F. & VAN BUCHEM, F. H. P (eds) *Cenozoic Sedimentary Basins of South Central Turkey. Sedimentary Geology, Special Issue*, **173**(1–4), 373–408.

PURVIS, M. & ROBERTSON, A. H. F. 2005*b*. Miocene sedimentary evolution of the NE–SW-trending Selendi and Gördes Basins, W Turkey: implications for extensional processes. *Sedimentary Geology*, **174**, 31–62.

ROBERTSON, A. H. F. & DIXON, J. E. 1984. Introduction: aspects of the geological evolution of the eastern Mediterranean. *In*: DIXON, J. E. & ROBERTSON, A. H. F. (eds) *The Evolution of the Eastern Mediterranean*. Geological Society, London, Special Publications, **17**, 1–74.

ŞENEL, M. 1997*a*. *Geological maps of Turkey in 1:100 000 scale: Fethiye L8 sheet*. Mineral Research and Exploration Directorate of Turkey (MTA), Ankara.

ŞENEL, M. 1997*b*. *Geological maps of Turkey in 1:100 000 scale: Fethiye M8 sheet*. Mineral Research and Exploration Directorate of Turkey (MTA), Ankara.

ŞENEL, M. 1997*c*. *Geological maps of Turkey in 1:100 000 scale: Denizli K9 sheet*. Mineral Research and Exploration Directorate of Turkey (MTA), Ankara.

ŞENEL, M. 1997*d*. *Geological maps of Turkey in 1:250 000 scale: Isparta sheet*. Mineral Research and Exploration Directorate of Turkey (MTA), Ankara.

ŞENEL, M. 1997*e*. *Geological maps of Turkey in 1:250 000 scale: Antalya sheet*. Mineral Research and Exploration Directorate of Turkey (MTA), Ankara.

ŞENEL, M. 1997*f*. *Geological maps of Turkey in 1:250 000 scale: Fethiye sheet*. Mineral Research and Exploration Directorate of Turkey (MTA), Ankara.

ŞENGÖR, A. M. C. 1987. Cross-faults and differential stretching of hanging walls in regions of low angle normal faulting; examples from western Turkey. *In*: COWARD, M. P., DEWEY, J. F. & HANCOCK, P. L. (eds) *Continental Extensional Tectonics*. Geological Society, London, Special Publications, **28**, 575–589.

ŞENGÖR, A. M. C. & YILMAZ, Y. 1981. Tethyan evolution of Turkey: a plate tectonic approach. *Tectonophysics*, **75**, 181–241.

ŞENGÖR, A. M. C., GÖRÜR, N. & ŞAROĞLU, F. 1985. Strike-slip faulting and related basin formation in zones of tectonic escape: Turkey as a case study. *In*: BIDDLE, K. T. & CHRISTIE BLICK, N. (eds) *Strike-Slip and Basin Formation*. SEPM (Society for Sedimentary Geology) Special Publications, **37**, 227–264.

SEYITOĞLU, G. & SCOTT, B. C. & RUNDLE, C. C. 1996. Timing of Cenozoic extensional tectonics in west Turkey. *Journal of the Geological Society, London*, **149**, 533–538.

TAYMAZ, T. & PRICE, S. P. 1992. The 12.05.1971 Burdur earthquake sequence, a synthesis of seismological and geological observations. *Geophysical Journal International*, **108**, 589–603.

TAYMAZ, T., JACKSON, J. & MCKENZIE, D. 1991. Active tectonics of the north and central Aegean Sea. *Geophysical Journal International*, **106**, 433–490.

TEMIZ, H., POISSON, A., ANDRIEUX, J. & BARKA, A. 1997. Kinematics of the Plio-Quaternary Burdur–Dinar cross-fault system in SW Anatolia (Turkey). *Annales Tectonicae*, **11**, 102–113.

TEMIZ, H., POISSON, A. & ANDRIEUX, J. 2001. The Plio-Quaternary extensional system of the western side of the Isparta angle in SW Turkey. *In*: *4th International Symposium on Eastern Mediterranean Geology, Isparta, Turkey*, 125–129.

TEN VEEN, J. H. 2004. Extension of Hellenic forearc shear zones in SW Turkey: the Pliocene–Quaternary deformation of the Eşen Çay Basin. *Journal of Geodynamics*, **37**, 181–204.

TEN VEEN, J. H. & KLEINSPEHN, K. L. 2002. Geodynamics along an increasingly curved convergent plate margin: Late Miocene–Pleistocene Rhodes (Greece). *Tectonics*, **21**, 10.1029/2001TC001287.

TEN VEEN, J. H. & KLEINSPEHN, K. L. 2003. Incipient continental collision and plate-boundary curvature: Late Pliocene–Holocene transtensional Hellenic forearc, Crete, Greece. *Journal of the Geological Society, London*, **160**, 161–181.

TEN VEEN, J. H. & POSTMA, G. 1999. Roll-back controlled vertical movements of outer-arc basins of the Hellenic subduction zone (Crete, Greece). *Basin Research*, **11**, 243–266.

TEN VEEN, J. H., WOODSIDE, J. M., ZITTER, T. A. C., DUMONT, J. F., MASCLE, J. & VOLKONSKAIA, A.

2004. Neotectonic evolution of the Anaximander Mountains at the junction of the Hellenic and Cyprus arcs. *Tectonophysics*, **391**, 35–65.

WESTAWAY, R. 1990. Block rotations in Western Turkey, 1. Observational evidence. *Journal of Geophysical Research, B*, **95**, 19857–19884.

WESTAWAY, R., PRINGLE, M., YURTMEN, S., DEMIR, T., BRIDGLAND, D., ROWBOTHAM, G. & MADDY, D. 2003. Pliocene and Quaternary surface uplift of western Turkey revealed by long-term river terrace sequences. *Current Science*, **84**(8), 1090–1101.

YILMAZ, Y., GENÇ, Ş. C., GÜRER, F., *et al.* 2000. When did the western Anatolian grabens begin to develop? *In*: BOZKURT, E., WINCHESTER, J. A. & PIPER, J. D. A. (eds) *Tectonics and Magmatism in Turkey and the Surrounding Area*. Geological Society, London, Special Publications, **173**, 353–384.

ZANCHI, A., KISSEL, C. & TAPIRDAMAZ, C. 1993. Late Cenozoic and Quaternary brittle continental deformation in western Turkey. *Bulletin de la Société Géologique de France*, **164**, 507–517.